<Electronic Supplementary Information>

New topological 3D copper(II) coordination networks: catechol oxidation catalysis and solvent adsorption via porous properties

Doeon Kim, Byung Joo Kim, Tae Hwan Noh and Ok-Sang Jung*

Department of Chemistry, Pusan National University, Pusan 609-735, Korea

Refinements of structures with the SQUEEZE routine in PLATON.

For the present copper(II) complexes, the simple solvate molecules of both complexes and the anions in case of $[Cu_3L_4(CH_3CN)_6](BF_4)_6 \cdot 16H_2O \cdot 5CH_3CN$ in the voids were highly disordered and were impossible to refine using conventional discrete-atom models. Therefore, the residual electron density was treated as diffuse contributions using the SQUEEZE of the PLATON software and located a series of voids (see below).[1]

For **$[Cu_3L_4(CH_3CN)_6](ClO_4)_6 \cdot 19H_2O \cdot 6CH_3CN$**,

_platon_squeeze_void_nr
 _platon_squeeze_void_average_x
 _platon_squeeze_void_average_y
 _platon_squeeze_void_average_z
 _platon_squeeze_void_volume
 _platon_squeeze_void_count_electrons
 _platon_squeeze_void_content

1	0.304	0.376	0.054	2675	860 ''
2	0.804	0.876	0.054	2675	860 ''
3	0.500	0.890	0.250	76	32 ''
4	1.000	0.390	0.250	76	32 ''
5	0.500	0.110	0.750	76	32 ''

6 1.000 0.610 0.750   76   32''
_platon_squeeze_details
;

For **[Cu₃L₄(CH₃CN)₆](BF₄)₆·16H₂O·5CH₃CN**,

_platon_squeeze_void_nr
 _platon_squeeze_void_average_x
 _platon_squeeze_void_average_y
 _platon_squeeze_void_average_z
 _platon_squeeze_void_volume
 _platon_squeeze_void_count_electrons
 _platon_squeeze_void_content
  1 0.003 -0.004 -0.015   6993   2368''
_platon_squeeze_details
;

References for X-ray Crystallography:

1   A. L. Spek, *J. Appl. Crystallogr.*, 2003, **36**, 7-13.
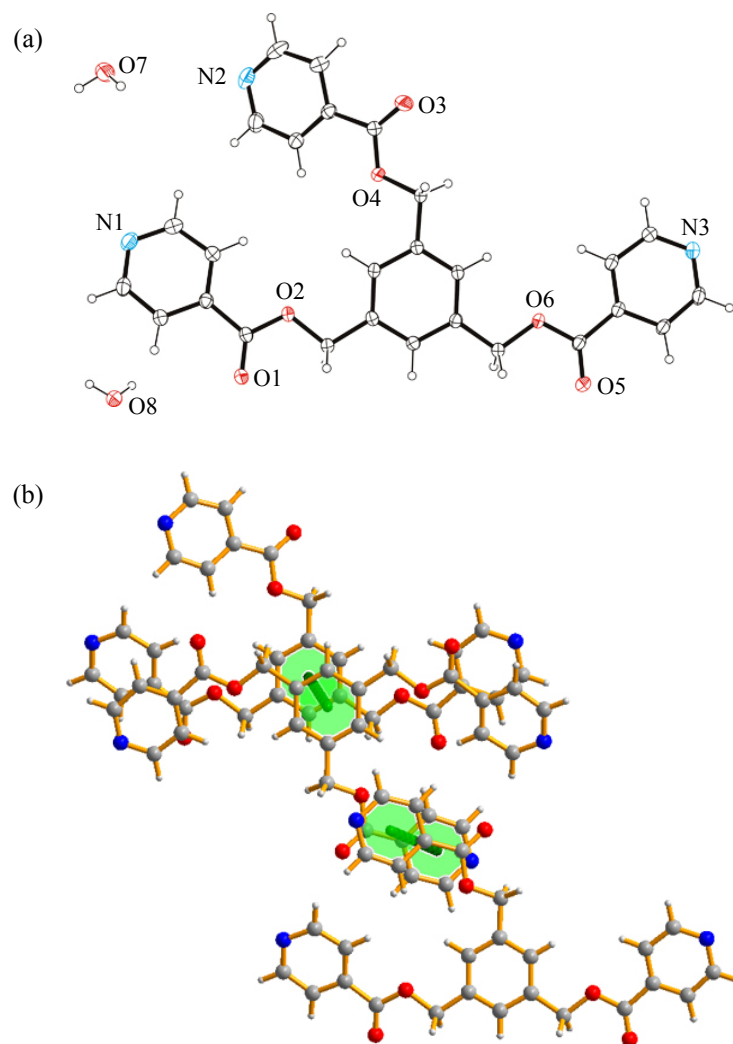
Fig. S1 Crystal structure of L: ORTEP drawing with anisotropic displacement parameters at 30% probability (a) and partial packing diagram showing highlighted intermolecular $\pi\cdots\pi$ interactions (b).
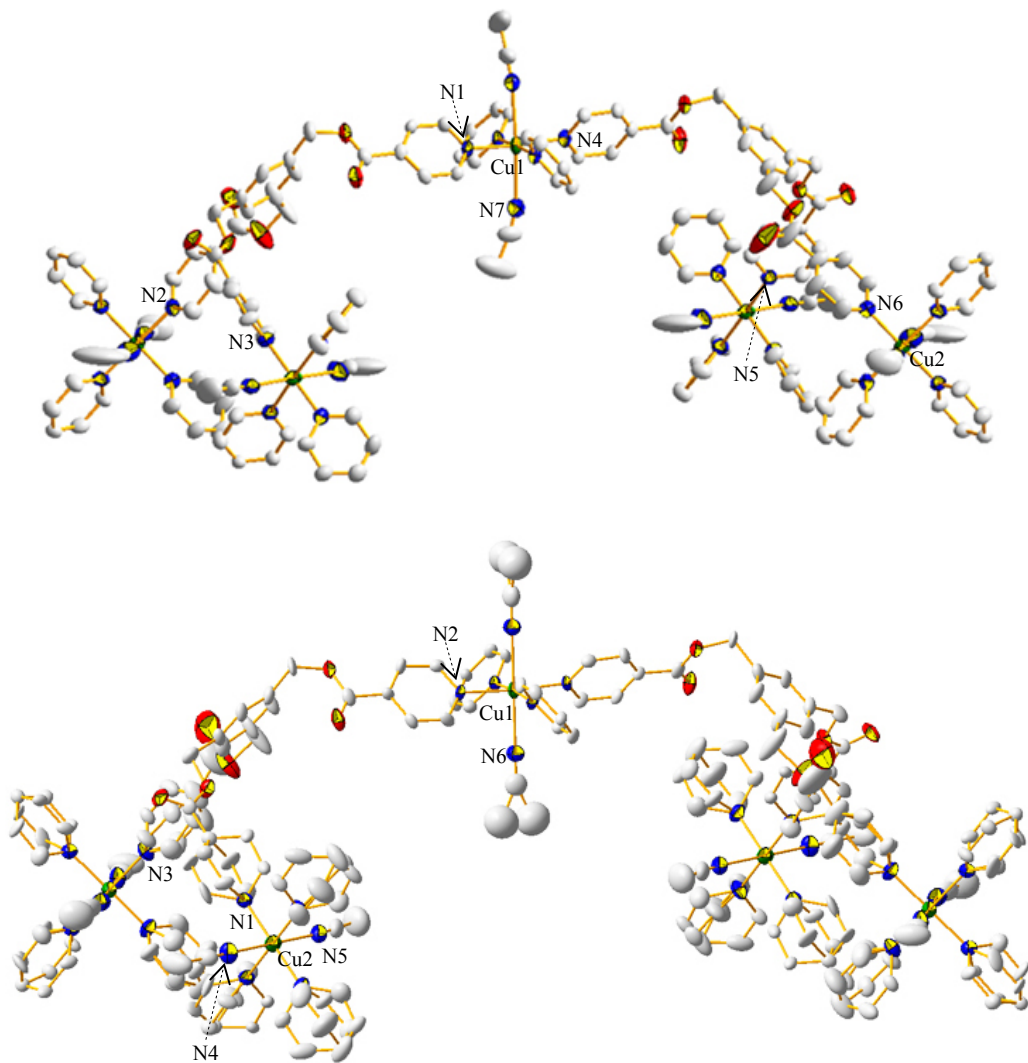
Fig. S2 X-ray crystal structure of [Cu₃L₄(CH₃CN)₆](ClO₄)₆·19H₂O·6CH₃CN (top) and

[Cu₃L₄(CH₃CN)₆](BF₄)₆·16H₂O·5CH₃CN (bottom) with anisotropic displacement parameters at

30% and 20% probabilities, respectively. The hydrogen atoms and counteranions were omitted

for clarity.

(a) (b)
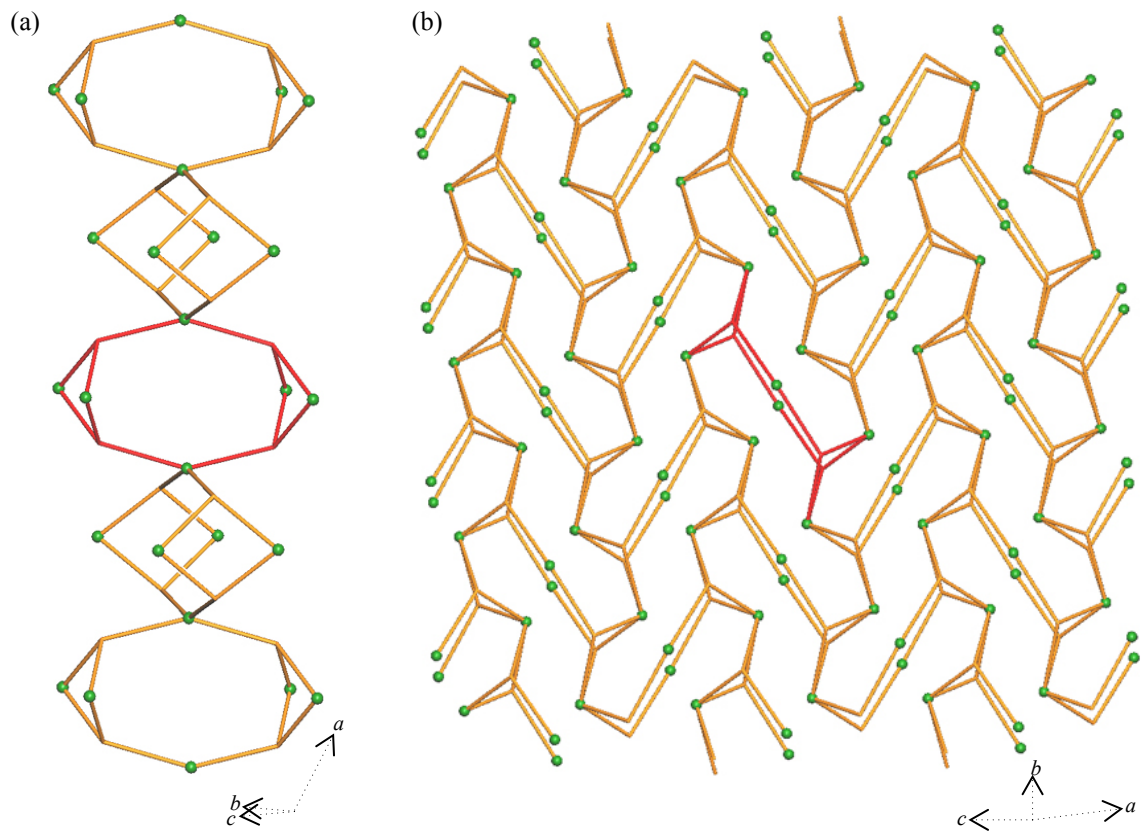
Fig. S3 Schematic representation showing linkage of the subunits connected through Cu(1) to form 1D linked cages running perpendicular to the *bc*-plane (a) and linked through Cu(2) in the crystallographic *bc*-direction (b).
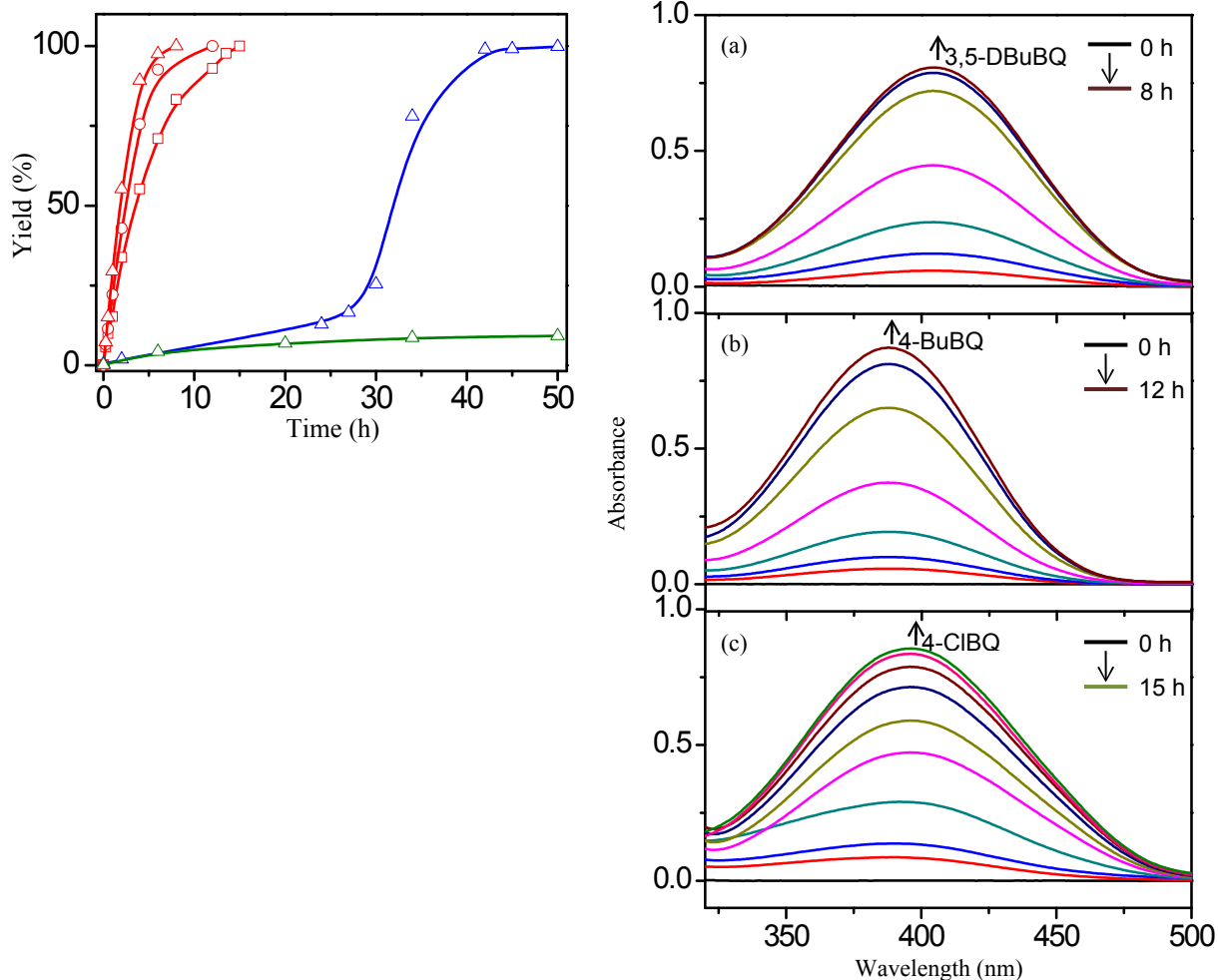
Fig. S4 Left: plot showing catalytic yields of 3,5-DBuCat (triangles), 4-BuCat (circles), and 4-ClCat (squares) using $[Cu_3L_4(CH_3CN)_6](ClO_4)_6 \cdot 19H_2O \cdot 6CH_3CN$ (red lines), mixture of $Cu(ClO_4)_2$ and L in 3 : 4 ratio (blue line), and only $Cu(ClO_4)_2$ (green line) as catalysts. The [catalyst] : [catechol] ratio is 1 : 1 in $CHCl_3$ at 40 °C. Right: UV/vis spectra showing oxidation of 3,5-DBuCat (a), 4-BuCat (b), and 4-ClCat (c) using $[Cu_3L_4(CH_3CN)_6](ClO_4)_6 \cdot 19H_2O \cdot 6CH_3CN$ as a catalyst. The [catalyst] : [catechol] ratio is 1 : 1.
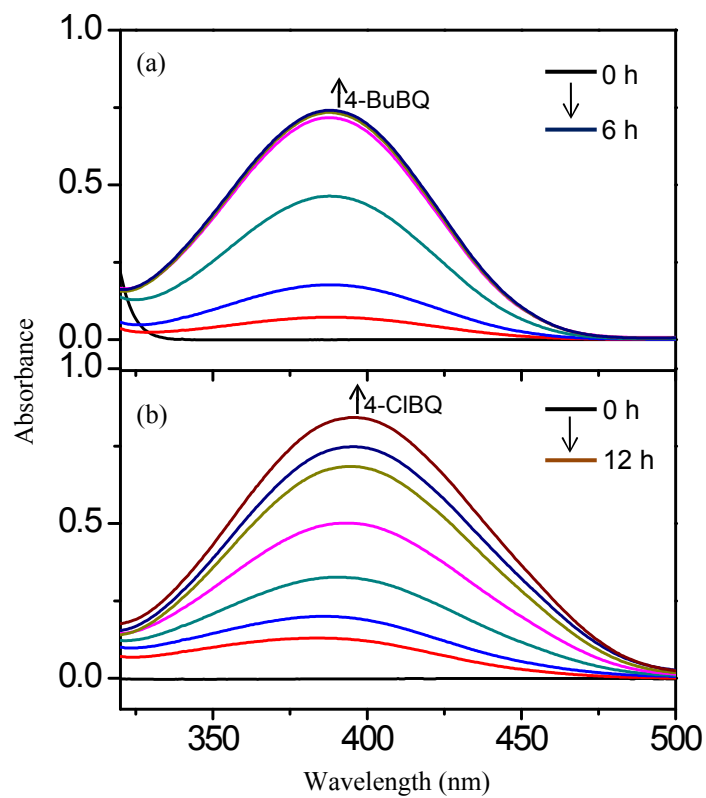
Fig. S5 UV/vis spectra showing the oxidation of 4-BuCat (a) and 3-ClCat (b) using [Cu$_3$L$_4$(CH$_3$CN)$_6$](BF$_4$)$_6$·16H$_2$O·5CH$_3$CN as acatalyst. The [catalyst] : [catechol] ratio is 1 : 1 in CHCl$_3$ at 40 °C.
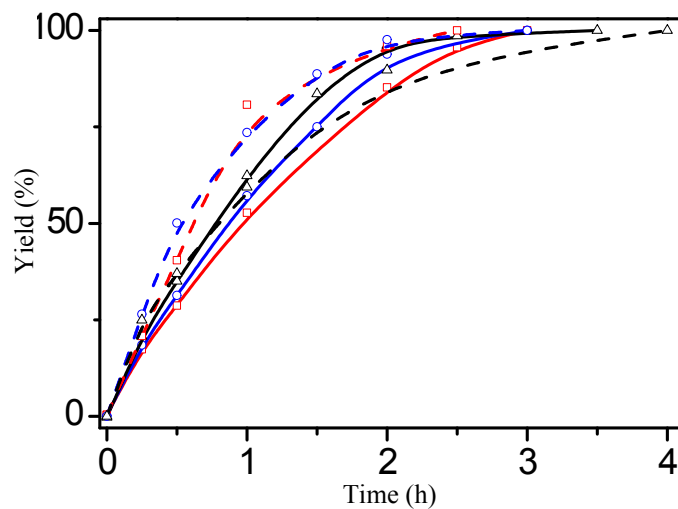
Fig. S6 Plot showing catalytic yields of 3,5-DBuCat (red), 4-BuCat (blue), and 4-ClCat (black) using $[Cu_3L_4(CH_3CN)_6](ClO_4)_6 \cdot 19H_2O \cdot 6CH_3CN$ (solid lines) and

$[Cu_3L_4(CH_3CN)_6](BF_4)_6 \cdot 16H_2O \cdot 5CH_3CN$ (dashed lines) as catalysts. The [catalyst] : [catechol] ratio is 2 : 1 in $CHCl_3$ at 40 °C.
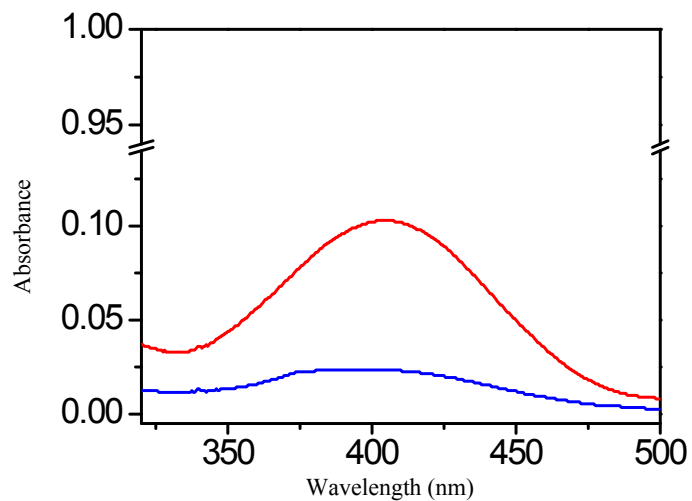
Fig. S7 UV/vis spectra showing oxidation of 3,5-DBuCat using CuCl$_2$ (red) and CuO (blue) as catalysts in CHCl$_3$ at 40 °C. The catalytic yields are 12% and 3% for 24 h, respectively.
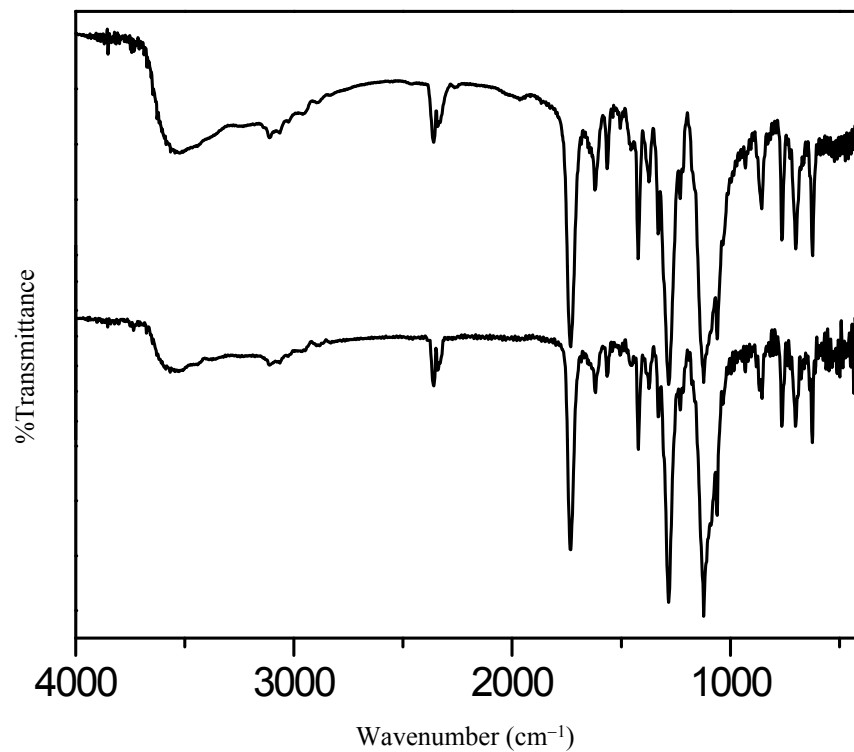
Fig. S8 IR spectra of $[Cu_3L_4(CH_3CN)_6](ClO_4)_6 \cdot 19H_2O \cdot 6CH_3CN$ before (top) and after (bottom) catechol oxidation catalysis of 3,5-DBuCat.
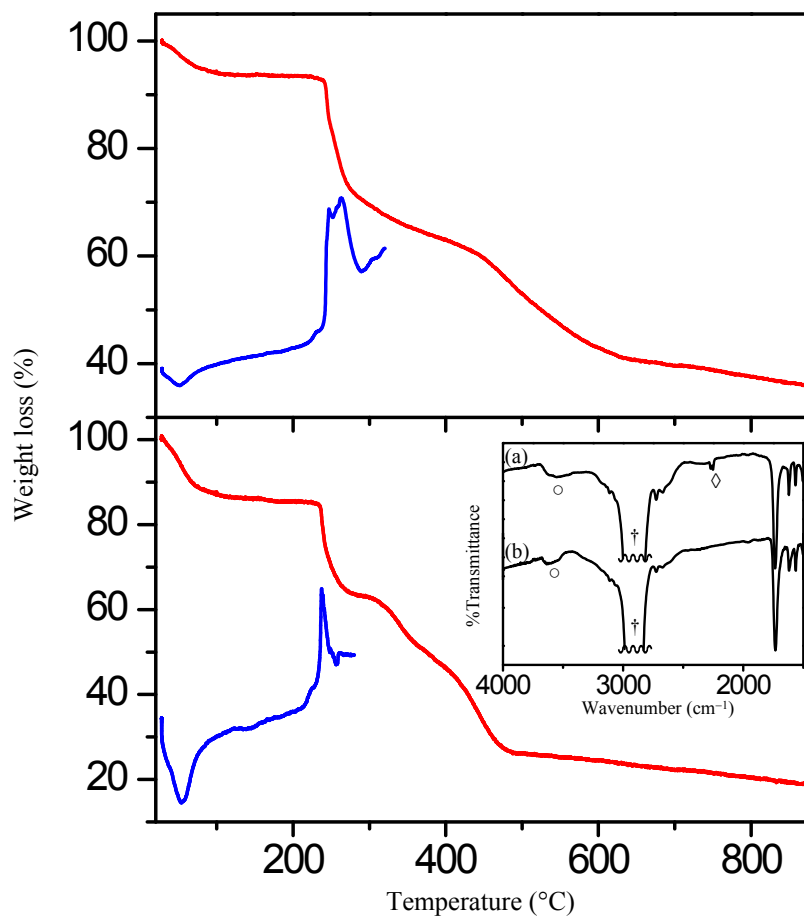
Fig. S9 TGA (red lines) and DSC (blue lines) curves of

$[Cu_3L_4(CH_3CN)_6](ClO_4)_6 \cdot 19H_2O \cdot 6CH_3CN$ (top) and $[Cu_3L_4(CH_3CN)_6](BF_4)_6 \cdot 16H_2O \cdot 5CH_3CN$

(bottom). Inset: IR spectra (Nujol mull) of as-synthesized samples (a) and acetonitrile-desolvated

samples (b). The circle, rhombus, and dagger denote the vibrational frequencies corresponding to

$\tilde{v}_{OH}$ of water, $\tilde{v}_{C\equiv N}$ of acetonitrile, and the sp^3 hydrocarbon of Nujol, respectively.
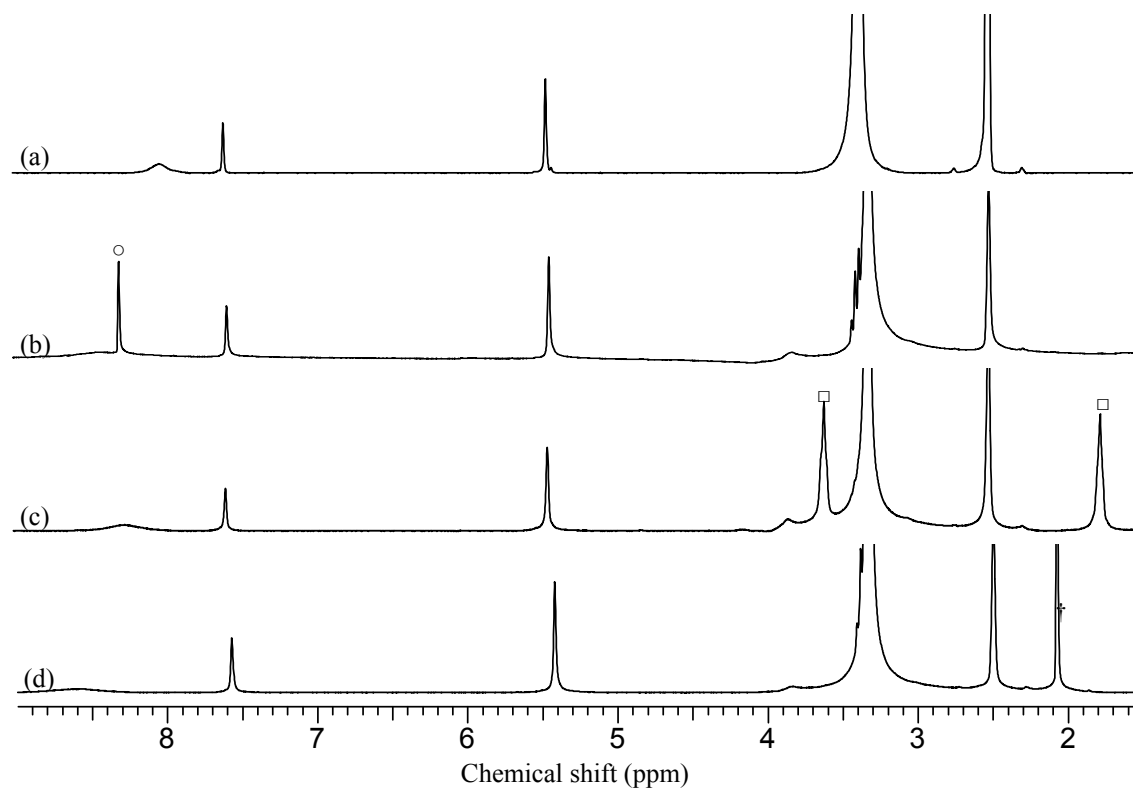
Fig. S10 ^{1}H NMR (Me$_2$SO-d_6) spectra for the acetonitrile-desolvated [Cu$_3$L$_4$](ClO$_4$)$_6$·19H$_2$O (a), and reincorporated samples [Cu$_3$L$_4$](ClO$_4$)$_6$·19H$_2$O·12CHCl$_3$ (b), [Cu$_3$L$_4$](ClO$_4$)$_6$·19H$_2$O·13THF (c), and [Cu$_3$L$_4$](ClO$_4$)$_6$·19H$_2$O·7Me$_2$CO (d). The circle, squares, and dagger denote the resonances of CHCl$_3$, THF, and acetone, respectively.
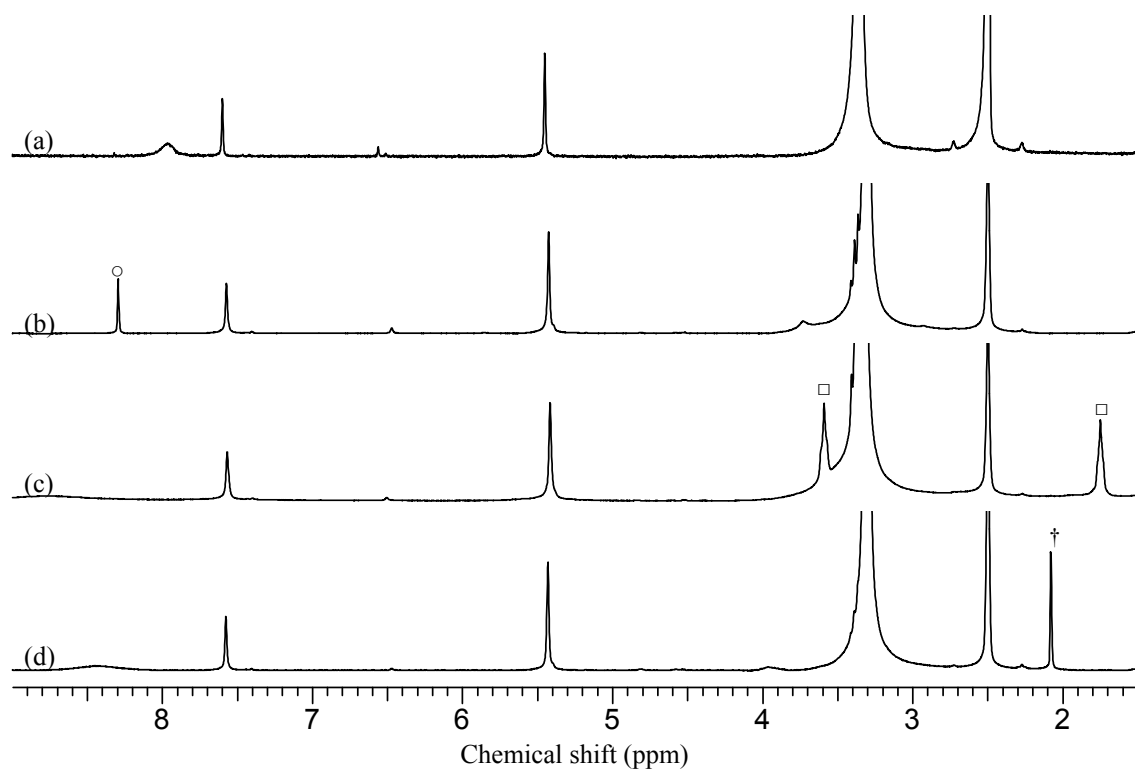
Fig. S11 ^{1}H NMR (Me$_2$SO-d_6) spectra for the acetonitrile-desolvated [Cu$_3$L$_4$](BF$_4$)$_6$·16H$_2$O (a),

and reincorporated samples [Cu$_3$L$_4$](BF$_4$)$_6$·16H$_2$O·7CHCl$_3$ (b), [Cu$_3$L$_4$](BF$_4$)$_6$·16H$_2$O·8THF (c),

and [Cu$_3$L$_4$](BF$_4$)$_6$·16H$_2$O·4Me$_2$CO (d). The circle, squares, and dagger denote the resonances of

CHCl$_3$, THF, and acetone, respectively.
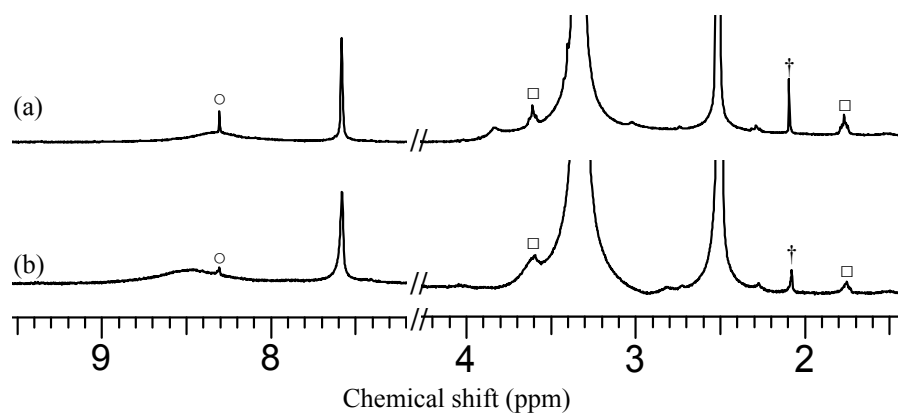
Fig. S12 ^{1}H NMR (Me$_2$SO-d_6) spectra representing the solvent-adsorption ratio of

[Cu$_3$L$_4$](ClO$_4$)$_6$·19H$_2$O (a) and [Cu$_3$L$_4$](BF$_4$)$_6$·16H$_2$O (b) by immersing in a mixture of CHCl$_3$,

THF, and acetone ($v/v/v$ = 1:1:1). The circles, squares, and daggers denote the resonances of

CHCl$_3$, THF, and acetone, respectively.